Physical properties and structural chemistry of $Ce(Ni_{1-x}Ga_x)_5$ alloys

H. Flandorfer, P. Rogl,* and K. Hiebl
Institut für Physikalische Chemie der Universität Wien, A-1090 Wien, Währingerstrasse 42, Austria

E. Bauer, A. Lindbaum, and E. Gratz
Institut für Experimentalphysik der Technischen Universität Wien, A-1040 Wien, Wiedner Hauptstrasse 8-10, Austria

C. Godart
CNRS, Laboratoire de Chimie Métallurgique des Terres Rares, Equipe de Recherche 209, Place Aristide Briand, 92195 Meudon Cedex, France
and Laboratoire pour l'Utilisation du Rayonnement Electromagnetique, Université de Paris Sud, 91405 Orsay, France

D. Gignoux and D. Schmitt
CNRS, Grenoble, Laboratoire Louis Néel, F-3842 Grenoble Cedex, France
(Received 16 August 1993; revised manuscript received 20 June 1994)

The $Ce(Ni_{1-x}Ga_x)_5$ system has been investigated in the range from $x=0$ to $x\sim0.6$ including measurements of (a) the lattice parameters at room temperature and down to 4 K on samples quenched from 600 or 800 °C, respectively, (b) the magnetic susceptibility in the temperature range $1.5 < T < 800$ K and magnetization measurements up to 8 T, (c) the electrical resistivity from 4.2 to 300 K, (d) the specific heat from 1.5 to 60 K and (e) x-ray absorption spectroscopy (XAS) and x-ray absorption near-edge structure (XANES) at 10 and ~290 K. At 800 °C, a continuous solid solution $0 \le x \le 0.55$ is observed crystallizing with the $CaCu_5$ type. Within this solution range a $HoNi_{2.6}Ga_{2.4}$-type low-temperature modification develops with a small homogeneity range around $CeNi_3Ga_2$ and with a maximum congruent transformation point at $T \cong 770$ °C. The Ni/Ga substitution leads to a successive occupation of the 3*g* sites of *P6/mmm* symmetry by Ga, whereas the 2*c* sites are Ga free, but ultimately does not reach full atomic order at a hypothetical "$CeNi_2Ga_3$." Magnetism within the solid solution starts with a nonmagnetic ground state of the cerium atoms in $CeNi_5$ but subsequently changes to an intermediate Ce valence as the Ga content increases. $CeNi_3Ga_2$ in the low-temperature modification exhibits Curie-Weiss behavior and enhanced values for the electronic contribution to the specific heat as typically observed for heavy-fermion compounds. The Ce valency, directly obtained from XAS data, shows a linear decrease as a function of increasing Ni/Ga substitution, with a strong temperature dependence for the alloy richest in Ga, $CeNi_{2.34}Ga_{2.66}$. The linear variation of the unit-cell parameters for (Y,La)-substituted alloys $Ce_{1-x}(Y,La)_xNi_3Ga_2$ in both structure modifications and the corresponding magnetic and XAS data revealed practically no influence on the cerium valence compared to the $CeNi_3Ga_2$ base alloys.

I. INTRODUCTION

Among highly correlated electron systems so-called heavy-fermion superconductors (HFS's) have recently received enhanced attention.[1,2] It is interesting to note, that those HFS's with the highest transition temperature exhibit the $CaCu_5$ type of structure.[3,4] Whereas these $CaCu_5$-type HFS systems have been observed with ternary uranium aluminides,[3,4] no corresponding HFS system so far is known for cerium alloys, although peculiar low-temperature properties have been found for a couple of substituted Ce compounds based on this hexagonal structure.[5] This particularly triggered our present interest in the Ce-Ni-Ga alloy system. From an earlier investigation of the phase relations and crystal structures in an isothermal section of the ternary system Ce-Ni-Ga at 600 °C,[6,7] the existence of phases with the $CaCu_5$ type and a derivative type ($HoNi_{2.6}Ga_{2.4}$) have been reported. From these investigations at 600 °C, employing x-ray powder-diffraction techniques and microscopic inspection, the authors of Refs. 6 and 7 claimed the formation of an extended solid solution of Ga in binary $CeNi_5$ up to about 25 at. % Ga and, furthermore, the formation of a $HoNi_{2.6}Ga_{2.4}$-type phase with a small homogeneity range, $CeNi_{3.07-2.83}Ga_{1.93-2.17}$, as well as a second $CaCu_5$-type phase but with a smaller homogeneity range at higher Ga concentrations, $CeNi_{2.53-2.23}Ga_{2.47-2.77}$. Except for a preliminary investigation of the electrical resistivity and the thermoelectric power above about 77 K,[8,9] no physical properties of $Ce(Ni_{1-x}Ga_x)_5$ alloys have been reported in literature.

From the type of data reported in Refs. 6 and 7 we expect a continuous solid solution for the $CaCu_5$ type for the entire range up to $CeNi_2Ga_3$ at temperatures above 600 °C; in this case the intermediate solid solution phase $CeNi_{\sim3}Ga_{\sim2}$ with the $HoNi_{2.6}Ga_{2.4}$ type will appear as a low-temperature compound exhibiting a congruent transformation at a maximum transition point where it trans-

forms to the $CaCu_5$ type. In order to confirm this hypotheses, a systematic investigation of the phase relations and crystal chemistry along the isopleth $Ce(Ni_{1-x}Ga_x)_5$ at temperatures $\geq 600\,^{\circ}C$ became the subject of the present work aimed at a thorough study of the physical properties as a function of the Ni/Ga ratio using electrical resistivity, magnetic susceptibility, magnetization, specific heat, as well as CeL_{III} x-ray-absorption spectroscopy to monitor eventual Ce-valence instabilities or HFS behavior. To simulate the pressure dependence of the physical properties, use is made of the internal chemical pressure in the crystallographic unit cell on substitution of the cerium atoms by larger lanthanum atoms or by much smaller yttrium atoms.

II. EXPERIMENT

The samples with nominal compositions along the $CeNi_5$-$CeGa_5$ system, each with a total weight of $\sim 1.5-2$ g, have been prepared from the elements by argon arc melting (see Table I). The starting materials used were ingots of cerium with a nominal purity of 99.9 mass % from Auer Remy, FRG, gallium (purity 99.99 mass %) from Alcan Electronics, Switzerland and pellets of nickel which were premelted from proper amounts of compacted nickel powder with a nominal purity of 99.9 mass %, PRC, USA. In order to ensure homogeneity, the samples were remelted several times. Weight losses due to vaporization were generally less than 1 mass %. The reguli obtained were wrapped in protective Mo foil, sealed in evacuated silica tubes, and heat treated at various temperatures in the range from 600 to 800 °C (168 h). After annealing in a wire-wound power-controlled tubular furnace calibrated against a Pt/PtRh thermocouple, the samples were quenched in cold water. Precise lattice parameters and standard deviations were obtained by a least-squares refinement of room temperature Guinier-Huber x-ray (Cu $K\alpha_1$) powder data employing an internal standard of 99.9999 mass % pure germanium ($a_{Ge}=0.565\,790\,6$ nm). For quantitative refinement of the atom positions either the x-ray intensities were recorded from a flat specimen in a Siemens D5000 automatic powder diffractometer (Cu $K\alpha$) or intensity data were read from Guinier-Huber photographs (Cu $K\alpha_1$) employing a computer controlled LS20-laser linescanner.[10] Full matrix/full profile Rietveld refinements have been performed employing a PC version of the program by Wiles and Young.[11]

The temperature dependence of the unit-cell dimensions in the temperature range from 4.2 to 300 K has been recorded on a Siemens D500 automatic diffractrometer, (Co $K\alpha$) with the flat sample mounted in an evacuated Oxford Instruments helium-flow cryostat. Lattice parameters at each temperature have been derived by a least-squares refinement assuming a Lorentzian peak shape and calibrating against Ge-standard lines.[12]

To check microstructure and homogeneity, selected alloys have been subjected to metallographic analysis of polished surfaces. Homogeneity was confirmed for $CeNi_{2.34}Ga_{2.66}$ for which detailed magnetic and x-ray-absorption spectroscopy (XAS) data have been calculated. Magnetic measurements have been performed with a Lake Shore ac susceptometer down to liquid-helium temperature. For temperatures above liquid nitrogen up to 800 K, a Faraday balance SUS-10 was used. Isothermal magnetization measurements in fields up to 8 T have been performed in an extraction magnetometer.

X-ray-absorption measurements were performed at the French synchrotron radiation facility of LURE using the x-ray beam delivered by the DCI storage ring, working at 1.85 GeV, ~ 320 mA, on the extended x-ray-absorption fine-structure 2 station. A double Si(311) crystal was used as a monochromator. Rejection of harmonics of order 3 was achieved by two parallel mirrors adjusted to cut off higher energies than ~ 9 keV in the incident beam. Experiments were made in the range 5660–5840 eV around the L_{III} edge of cerium. Powdered samples were spread on adhesive Kapton tape, and three such tapes were stacked to make a sufficiently thick sample to provide the expected amplitude of the discontinuity as well as to avoid any discontinuities in the powder distribution. Samples were also measured in a cryostat kept at a constant temperature of ~ 10 K. After subtracting the background from the spectra in a standard manner, L_{III}-edge deconvolution was made using a technique already described,[13] with a PC computer program.[14]

Resistivity measurements on bar-shaped samples were performed using a standard dc 4-wire technique. Specific-heat data were taken from a fully automated Nernst calorimeter in a temperature range from 1.5 to 60 K.

III. RESULTS AND DISCUSSION

A. Compound formation and phase equilibria

X-ray powder analyses of the alloys along the $CeNi_5$-$CeGa_5$ system, annealed at 600 °C, confirmed the phase relations earlier described by Refs. 6 and 7. Our results particularly refer to the formation of an extended solid solution, $Ce(Ni_{1-x}Ga_x)_5$, $0 \leq x \leq 0.3$, with the $CaCu_5$ type and the existence of a $CaCu_5$-derivative type, $CeNi_{3.07-2.83}Ga_{1.93-2.17}$, with the $HoNi_{2.6}Ga_{2.4}$ type (see Table I). At higher Ga concentrations, the $CaCu_5$ type reappears for compositions $CeNi_{2.53-2.23}Ga_{2.47-2.77}$. Whereas both two-phase fields $Ce(Ni,Ga)_5 + CeNi_{\sim 3}Ga_{\sim 2}$ were found to be somewhat smaller than originally reported at 600 °C,[6,7] lattice parameters are in good agreement (see Table I). The concentration dependence of the lattice parameters for the $CaCu_5$-type samples annealed at 600 °C are summarized in Fig. 1 revealing a monotonic increase in **a** as well as in V with a slight negative deviation from Vegard's rule. For convenient comparison, the unit-cell dimensions of the alloys with the $HoNi_{2.6}Ga_{2.4}$ type (actually a disordered version of the YNi_2Al_3 type)[15] have been converted in Fig. 1 to those based on the $CaCu_5$-type subunit using the relation $a(HoNi_{2.6}Ga_{2.4}) \equiv a\sqrt{3}(CaCu_5)$. In agreement with earlier observations, the $HoNi_{2.6}Ga_{2.4}$ type was encountered with a rather limited homogeneity range viz. $CeNi_{3.07-2.83}Ga_{1.93-2.17}$ (Fig. 3). Whereas the reduced a

TABLE I. Crystallographic data of $Ce(Ni_{1-x}Ga_x)_5$ alloys, in the region $0 \leq x \leq 0.6$.

Alloy nominal comp.	Heat treatment	Phase analysis	Structure type	Space group	Unit-cell dimensions (nm) a	c	V	c/a	Ref.
$CeNi_5$	600 °C	$CeNi_5$	$CaCu_5$	*P6/mmm*	0.4885(1)	0.4005(1)	0.08275	0.820	a
	800 °C	$CeNi_5$	$CaCu_5$	*P6/mmm*	0.4885(1)	0.4006(3)	0.08280	0.820	a
	800 °C				0.4887	0.4007	0.0829	0.820	18
$CeNi_{4.62}Ga_{0.38}$	600 °C	$CeNi_{4.62}Ga_{0.38}$	$CaCu_5$	*P6/mmm*	0.4906(1)	0.4033(1)	0.08408	0.822	a
	800 °C	$CeNi_{4.62}Ga_{0.38}$	$CaCu_5$	*P6/mmm*	0.4906(1)	0.4034(1)	0.08407	0.822	a
$CeNi_{4.32}Ga_{0.68}$	600 °C	$CeNi_{4.32}Ga_{0.68}$	$CaCu_5$	*P6/mmm*	0.4922(1)	0.4059(1)	0.08516	0.825	a
	800 °C	$CeNi_{4.32}Ga_{0.68}$	$CaCu_5$	*P6/mmm*	0.4922(1)	0.4058(1)	0.08512	0.825	a
$CeNi_4Ga$	600 °C	$CeNi_4Ga$	$CaCu_5$	*P6/mmm*	0.4945(1)	0.4075(2)	0.08630	0.824	a
	800 °C	$CeNi_4Ga$	$CaCu_5$	*P6/mmm*	0.4949(1)	0.4085(2)	0.08665	0.825	a
$CeNi_{3.66}Ga_{1.34}$	600 °C	$CeNi_{3.66}Ga_{1.34}$	$CaCu_5$	*P6/mmm*	0.5004(2)	0.4091(2)	0.08871	0.818	a
	800 °C	$CeNi_{3.66}Ga_{1.34}$	$CaCu_5$	*P6/mmm*	0.5005(1)	0.4092(1)	0.08879	0.818	a
$CeNi_{3.6}Ga_{1.4}$	600 °C	$CeNi_{3.6}Ga_{1.4}$	$CaCu_5$	*P6/mmm*	0.501(1)	0.4105(8)	0.0892	0.820	7
$CeNi_{3.36}Ga_{1.64}$	600 °C	$CeNi_{3.47}Ga_{1.53}$	$CaCu_5$	*P6/mmm*	0.5046(1)	0.4075(2)	0.08985	0.875	a
		$CeNi_{3.07}Ga_{1.93}$	$HoNi_{2.6}Ga_{2.4}$	*P6/mmm*	0.8746(3)	0.4203(4)	0.2784	0.481	a
	800 °C	$CeNi_{3.36}Ga_{1.64}$	$CaCu_5$	*P6/mmm*	0.5053(1)	0.4092(1)	0.09047	0.810	a
$CeNi_{3.2}Ga_{1.8}$	600 °C	$CeNi_{3.47}Ga_{1.53}$	$CaCu_5$	*P6/mmm*	0.5065(2)	0.4080(2)	0.09062	0.806	a
		$CeNi_{3.07}Ga_{1.93}$	$HoNi_{2.6}Ga_{2.4}$	*P6/mmm*	0.8769(1)	0.4189(1)	0.2790	0.478	a
	800 °C	$CeNi_{3.2}Ga_{1.8}$	$CaCu_5$	*P6/mmm*	0.5076(1)	0.4096(1)	0.09140	0.807	a
$CeNi_{3.1}Ga_{1.9}$	600 °C	$CeNi_{3.47}Ga_{1.53}$	$CaCu_5$	*P6/mmm*	Traces				
		$CeNi_{3.07}Ga_{1.93}$	$HoNi_{2.6}Ga_{2.4}$	*P6/mmm*	0.8788(2)	0.4184(1)	0.2799	0.476	a
	800 °C	$CeNi_{3.1}Ga_{1.9}$	$CaCu_5$	*P6/mmm*	0.5086(1)	0.4097(1)	0.09177	0.805	a
$CeNi_{3.05}Ga_{1.95}$	600 °C	$CeNi_{3.05}Ga_{1.95}$	$HoNi_{2.6}Ga_{2.4}$	*P6/mmm*	0.8791(2)	0.4180(1)	0.2798	0.476	a
	800 °C	$CeNi_{3.05}Ga_{1.95}$	$CaCu_5$	*P6/mmm*	0.5099(1)	0.4095(1)	0.09219	0.803	a
$CeNi_3Ga_2$	600 °C	$CeNi_3Ga_2$	$HoNi_{2.6}Ga_{2.4}$	*P6/mmm*	0.8800(1)	0.4183(1)	0.2805	0.475	a
	600 °C				0.882(1)	0.419(1)	0.2823	0.475	6,7
	600 °C				0.8762	0.4148	0.2758	0.473	17
	800 °C	$CeNi_3Ga_2$	$CaCu_5$	*P6/mmm*	0.5110(1)	0.4096(1)	0.09261	0.802	a
$CeNi_{2.9}Ga_{2.1}$	600 °C	$CeNi_{2.9}Ga_{2.1}$	$HoNi_{2.6}Ga_{2.4}$	*P6/mmm*	0.8817(2)	0.4178(2)	0.2813	0.474	a
	800 °C	$CeNi_{2.9}Ga_{2.1}$	$CaCu_5$	*P6/mmm*	0.5122(1)	0.4092(1)	0.0930	0.799	a
$CeNi_{2.8}Ga_{2.2}$	600 °C	$CeNi_{2.8}Ga_{2.2}$	$HoNi_{2.6}Ga_{2.4}$	*P6/mmm*	0.883(3)	0.421(3)	0.2843	0.477	7
$CeNi_{2.75}Ga_{2.25}$	600 °C	$CeNi_{2.53}Ga_{2.47}$	$CaCu_5$	*P6/mmm*	0.5196(1)	0.4073(2)	0.09522	0.784	a
		$CeNi_{2.83}Ga_{2.17}$	$HoNi_{2.6}Ga_{2.4}$	*P6/mmm*	0.8809(4)	0.4185(2)	0.2812	0.475	a
	800 °C	$CeNi_{2.75}Ga_{2.25}$	$CaCu_5$	*P6/mmm*	0.5150(0)	0.4086(1)	0.09384	0.793	a
$CeNi_{2.68}Ga_{2.32}$	600 °C	$CeNi_{2.53}Ga_{2.47}$	$CaCu_5$	*P6/mmm*	0.5187(1)	0.4072(1)	0.09488	0.785	a
		$CeNi_{2.83}Ga_{2.17}$	$HoNi_{2.6}Ga_{2.4}$	*P6/mmm*	0.8813(2)	0.4185(2)	0.2815	0.475	a
	800 °C	$CeNi_{2.68}Ga_{2.32}$	$CaCu_5$	*P6/mmm*	0.5167(1)	0.4079(1)	0.09430	0.789	a
$CeNi_{2.49}Ga_{2.51}$	600 °C	$CeNi_{2.49}Ga_{2.51}$	$CaCu_5$	*P6/mmm*	0.5193(1)	0.4075(1)	0.09517	0.785	a
$CeNi_{2.34}Ga_{2.66}$	600 °C	$CeNi_{2.34}Ga_{2.66}$	$CaCu_5$	*P6/mmm*	0.5232(2)	0.4058(2)	0.09618	0.776	a
	800 °C	$CeNi_{2.34}Ga_{2.66}$	$CaCu_5$	*P6/mmm*	0.5229(1)	0.4058(1)	0.09610	0.776	a
$CeNi_2Ga_3$	600 °C	$CeNi_{2.23}Ga_{2.77}$	$CaCu_5$	*P6/mmm*	0.5258(2)	0.4046(2)	0.09686	0.769	a
			$BaAl_4$	*I4/mmm*	0.4237(1)	1.0190(3)	0.18291	2.405	a
			$NaZn_{13}$	*Fm3̄c*	Traces				a
	600 °C	$CeNi_{2.2}Ga_{2.8}$	$CaCu_5$	*P6/mmm*	0.5263	0.4053	0.0972	0.770	6,7
		$CeNi_{1.1}Ga_{2.9}$	$BaAl_4$	*I4/mmm*	0.4234	1.0190	0.1827	2.407	6
		$CeNi_{5.7}Ga_{7.3}$	$NaZn_{13}$	*Fm3̄c*	1.1742		1.6189		6
	800 °C	$CeNi_{2.23}Ga_{2.77}$	$CaCu_5$	*P6/mmm*	0.5252(1)	0.4052(2)	0.09679	0.772	a
			$BaAl_4$	*I4/mmm*	0.4233(1)	1.0189(3)	0.18261	2.407	a
			$NaZn_{13}$	*Fm3̄c*	Traces				a
$LaNi_4Ga$	600 °C	$LaNi_4Ga$	$CaCu_5$	*P6/mmm*	0.5072(1)	0.4055(2)	0.09033	0.800	a
	600 °C	$LaNi_{3.8}Ga_{1.2}$			0.5104(8)	0.407(1)	0.0918	0.797	7
$LaNi_3Ga_2$	600 °C	$LaNi_3Ga_2$	$HoNi_{2.6}Ga_{2.4}$	*P6/mmm*	0.8910(2)	0.4182(1)	0.2875	0.469	a
	600 °C	$LaNi_{2.9}Ga_{2.1}$			0.8809(3)	0.420(2)	0.2823	0.477	7
	600 °C	$LaNi_3Ga_2$			0.8893	0.4169	0.2855	0.469	17

[a]This work.

parameter and the volume both scale well with the $CaCu_5$-type phase, the *c* axes of $CeNi_3Ga_2$ are significantly larger with respect to the $CaCu_5$ type reflecting subtle changes in atom coordination (see Fig. 1 and Sec. III B and Fig. 4). It is interesting to note, that there are no observable deviations from the ideal $CaCu_5$-type crystal symmetry, either for the gallium-poor $CaCu_5$-type phase range or for the gallium-rich range $Ce(Ni_{1-x}Ga_x)_5$, $0.49 \leq x \leq 0.55$. The existence of these two $CaCu_5$-type phase regions with an intermittent $HoNi_{2.6}Ga_{2.4}$-type phase at compositions around stoichiometric $CeNi_3Ga_2$ immediately suggests a continuous homogeneous $CaCu_5$-type region at elevated temperatures with a maximum congruent transition point for the stoichiometric low-temperature phase $CeNi_3Ga_2$. A continuous solid solution range $Ce(Ni_{1-x}Ga_x)_5$, $0 \leq x \leq 0.55$, indeed was obvious from alloys annealed at 800 °C (see Table I and Fig. 2). Lattice parameters versus gallium concentration for the alloys quenched from 800 °C, in close similarity to those at 600 °C, reveal a monotonic increase in the *a* parameter and the volume, whereas a flat maximum is obvious for the *c* parameter around the composition $CeNi_3Ga_2$ suggesting partial atomic order (see also Sec. III B, "Structural chemistry"). Extrapolation of the lattice parameter curves yields the estimated unit-cell dimensions for hypothetical $CeGa_5$.

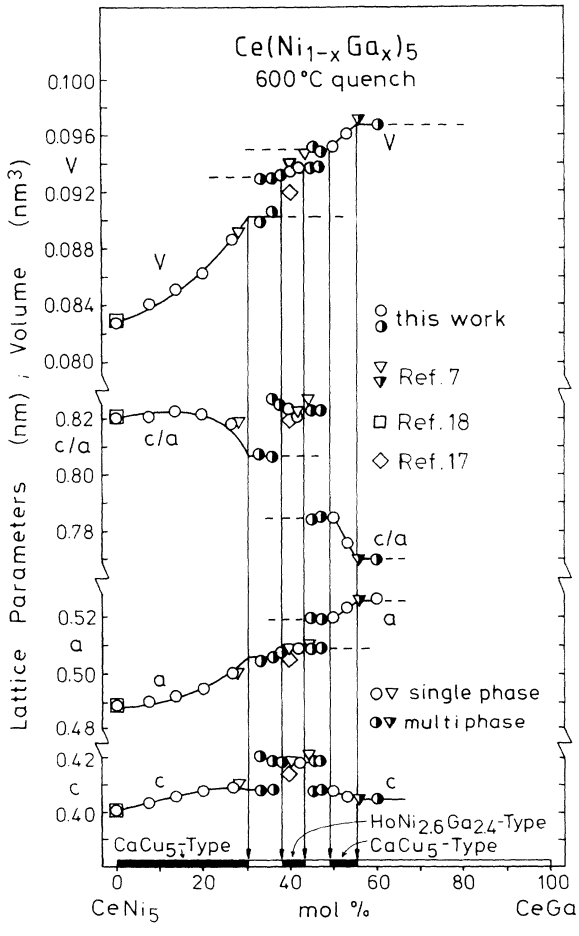

FIG. 1. Lattice parameters and volume of alloys $Ce(Ni_{1-x}Ga_x)_5$ versus composition. Alloys were quenched from 600 °C.

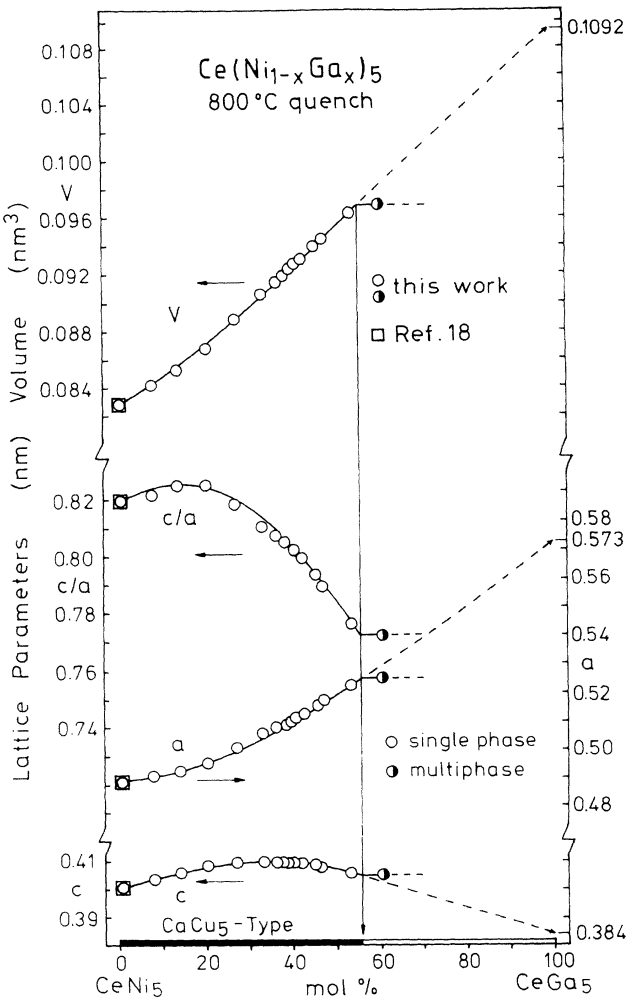

FIG. 2. Lattice parameters and volume of alloys $Ce(Ni_{1-x}Ga_x)_5$ versus composition. Alloys were quenched from 800 °C.

Figure 3 represents the phase relations along the nickel-rich part of the $Ce(Ni_{1-x}Ga_x)_5$ system, $0 \leq x \leq 0.6$, as derived from x-ray powder analysis of a

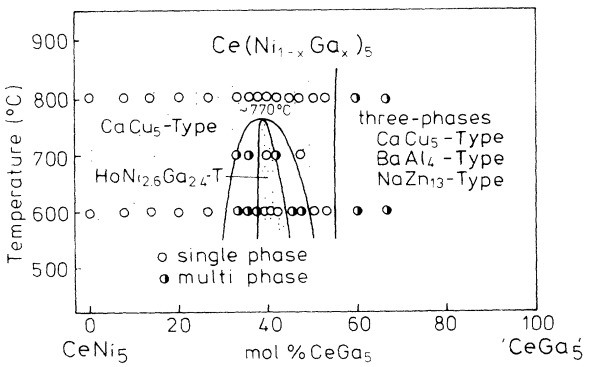

FIG. 3. Phase relations along the $CeNi_5$-$CeGa_5$ system at temperatures below 800 °C.

series of alloys quenched from 800, 700, and 600 °C, indicating a maximum congruent transformation point for $CeNi_3Ga_2$ with the $HoNi_{2.6}Ga_{2.4}$ type at about 770 °C. Due to the crystallographic relationship between the two structure types (see Sec. III B) the transformation process is controlled by diffusion. Therefore quenching the samples by submerging the quartz capsules in water proved to be sufficient in freezing the high-temperature phase into a metastable form at room temperature. Attempts to approach the composition $CeNi_2Ga_3$ by melt spinning, expected to provide a $CaCu_5$ type with full atom order but which proved to be stable in thermodynamic equilibrium at 800 °C, were unsuccessful. Experiments using a quartz nozzle and a water-cooled copper wheel at a speed of 24 ms^{-1} merely resulted in a heterogeneous mixture of three phases: $CaCu_5$ type, $BaAl_4$ type, and Fe_2P type.

B. Structural chemistry—Rietveld full profile refinements of x-ray powder data

Tables II and III summarize the results of the full-matrix, full-profile Rietveld refinements of the room-temperature x-ray powder intensities of $Ce(Ni_{0.80}Ga_{0.20})_5$, $Ce(Ni_{0.60}Ga_{0.40})_5$, and $Ce(Ni_{0.47}Ga_{0.53})_5$ with the $CaCu_5$ type and $Ce(Ni_{0.6}Ga_{0.4})_5$ with the $HoNi_{2.6}Ga_{2.4}$ type as collected from flat specimens in a D5000 Siemens automatic powder diffractometer. A major result of the refinement is that Ni atoms for all compositions investigated appear to favor the smaller $2c$ sites (Wyckoff symbol's) of $P6/mmm$ ($CaCu_5$ type), at the center points of (Ni,Ga) triangular prisms $[Ce_3(Ni,Ga)_6]Ni$. Gallium atoms preferentially occupy the slightly larger $3g$ sites. The least variation of interatomic distances as a function

TABLE II. Crystallographic data of $Ce(Ni_{1-x}Ga_x)_5$ alloys, quenched from 800 °C. Method: Full profile Rietveld refinement at room temperature x-ray powder-diffraction data (Siemens D5000); Space group: $P6/mmm$, $Z=1$; Structure type: $CaCu_5$; Radiation: Cu $K\alpha$.

Composition	$Ce(Ni_{0.8}Ga_{0.2})_5$	$Ce(Ni_{0.6}Ga_{0.4})_5$	$Ce(Ni_{0.47}Ga_{0.53})_5$
a (nm)	0.494 9(1)	0.511 0(1)	0.523 2(2)
c (nm)	0.408 5(2)	0.409 6(1)	0.405 8(2)
c/a	0.825	0.802	0.776
V (nm^3)	0.086 65(6)	0.092 61(6)	0.096 20(8)
$\sin\Theta_{max}/\lambda$, nm^{-1}	4.1724	4.3854	4.9725
No. of refl. in refin.	30	30	30
No. of variables	17	16	18
R_I	0.075	0.094	0.057
R_F	0.048	0.080	0.053
R_P	0.033	0.039	0.042
R_{wP}	0.047	0.055	0.054
Pref. orient.	0.130(5),‖(001)	−0.272(1),‖(001)	0.160(6),‖(100)
1 Ce in $1a$ (0,0,0)			
B in 10^{-2} nm^2	0.8(1)	0.1(−)	0.04(−)
2 Ni in $2c$ ($\frac{1}{3},\frac{2}{3},0$)			
B in 10^{-2} nm^2	1.6(1)	1.9(1)	0.37(4)
3 (Ni,Ga) in $3g$ ($\frac{1}{2},0,\frac{1}{2}$)	0.67Ni+0.33Ga	0.33Ni+0.67Ga	0.11Ni+0.89Ga
B in 10^{-2} nm^2	0.2(1)	0.06(−)	0.08(2)
Interatomic distances in nm			
Ce-2Ce	0.4085	0.4096	0.4059
Ce-6Ni	0.2857	0.2950	0.3020
Ce-12(Ni,Ga)	0.3209	0.3275	0.3311
Ni-3Ce	0.2857	0.2950	0.3020
Ni-6(Ni,Ga)	0.2492	0.2524	0.2530
(Ni,Ga)-4Ce	0.3209	0.3275	0.3311
(Ni,Ga)-4Ni	0.2492	0.2524	0.2530
(Ni,Ga)-4(Ni,Ga)	0.2476	0.2555	0.2616

TABLE III. Crystallographic data of $Ce(Ni_{0.6}Ga_{0.4})_5$, quenched from 600 °C.

Method: Full profile Rietveld refinement of room temperature x-ray powder-diffraction data. Number of reflections used in refinement: 57, $2\theta_{max}=93.00°$; Lattice parameters[a]: $a=0.8800(1)$ nm, $c=0.4183(1)$ nm, $V=0.2804(3)$ nm^3, $c/a=0.475$; Structure type: $HoNi_{2.6}Ga_{2.4}$ (disordered YNi_2Al_3 type); Space group: $P6/mmm$-D^1_{6h}, No. 191, origin at $\bar{1}$, $Z=3$; Residual values: $R_1=0.078$, $R_F=0.076$, $R_P=0.025$, $R_{wP}=0.035$.

		Atom parameters				
Atom	Site	x	y	z	$B(10^{-2}$ nm$^2)$	Occupation
Ce_1	1*a*	0	0	0	0.26(7)	1.0
Ce_2	2*d*	$\frac{1}{3}$	$\frac{2}{3}$	$\frac{1}{2}$	1.481(3)	1.0
$(Ga,Ni)_1$	3*f*	$\frac{1}{2}$	0	0	0.22(10)	b
$(Ga,Ni)_2$	6*k*	0.2825(3)	0	$\frac{1}{2}$	0.21(8)	b
Ni	6*l*	0.1785(4)	0.3570(4)	0.0	0.10(8)	1.0

Preferred orientation parameter: −0.07179(2), for (001)

Interatomic Distances up to 0.45 nm:

Ce_1-2Ce_1	0.4182	$(Ga,Ni)_2$-2Ce_1	0.3259
Ce_1-12$(Ga,Ni)_2$	0.3260	$(Ga,Ni)_2$-2$(Ga,Ni)_2$	0.2500
Ce_1-6Ni	0.2721	$(Ga,Ni)_2$-2$(Ga,Ni)_1$	0.2825
Ce_2-2Ce_2	0.4183	$(Ga,Ni)_2$-1$(Ga,Ni)_2$	0.3400
Ce_2-6$(Ga,Ni)_2$	0.3172	$(Ga,Ni)_2$-4Ni	0.2499
Ce_2-6$(Ga,Ni)_1$	0.3290	Ni-1Ce_1	0.2721
Ce_2-6Ni	0.3153	Ni-2Ce_2	0.3153
$(Ga,Ni)_1$-4Ce_2	0.3291	Ni-2$(Ga,Ni)_1$	0.2455
$(Ga,Ni)_1$-4$(Ga,Ni)_2$	0.2825	Ni-4$(Ga,Ni)_2$	0.2499
$(Ga,Ni)_1$-4Ni	0.2455	Ni-2Ni	0.2721
$(Ga,Ni)_2$-2Ce_2	0.3173		

[a]Lattice parameters derived from Guinierfilm.
[b]Occupation: (Ga,Ni)=0.67 Ga+0.33 Ni.

of increasing Ga content is the Ni-(Ni,Ga) contacts, indicating strong Ni-Ga interactions (see Table II). These interactions obviously constrain the lattice parameters and are held responsible for the occurrence of a maximum in the *c* parameter at about $Ce(Ni_{0.60}Ga_{0.40})_5$ (see Fig. 2). Further Ni/Ga substitution may finally yield the same structure as fully ordered $PrNi_2Al_3$,[16] an ordered variant of $CaCu_5$. It shall be noted, however, that the mode of Ga substitution observed herein is different from an earlier powder refinement of $CeNi_{2.2}Ga_{2.8}$ suggesting a random Ni,Ga atom distribution.[7] Refinement of the x-ray data for the low-temperature form of $CeNi_3Ga_2$ confirmed the $HoNi_{2.6}Ga_{2.4}$ type, which essentially is a disordered version of the fully ordered YNi_2Al_3 type.[15] The crystallographic relationship between the $CaCu_5$-type high-temperature form and the larger sized $HoNi_{2.6}Ga_{2.4}$-type low-temperature modification is outlined in Fig. 4. Due to the significant rearrangement of 33% of the cerium atoms, the center points of the triangular prisms in the $HoNi_{2.6}Ga_{2.4}$ type are occupied by nickel atoms in tetrakaidecahedral coordination $\{Ce(Ni,Ga)_2[Ce_2(Ni,Ga)_4]\}Ni$, whereas the remaining Ni atoms statistically share the 3*f* and 6*k* positions with Ga atoms (see also Table II). The observed partial (Ni,Ga) disorder, however, is in contradiction to the claimed isotypism of "$CeNi_3Ga_2$" with the fully ordered YCo_3Ga_2 type.[17]

C. Thermal expansion

Figure 5(a) portrays the variation of the unit-cell dimensions as a function of temperature (region from 4.2 to 300 K) for $CeNi_3Ga_2$ in the two modifications ($HoNi_{2.6}Ga_{2.4}$ type and $CaCu_5$ type), as well as for $CeNi_{2.34}Ga_{2.66}$ ($CaCu_5$ type). Emphasis has been laid on the low-temperature region below 50 K, and no significant indications for a low-temperature transition has become obvious from the recorded x-ray pattern (see also Sec. III F). In all cases the unit-cell dimensions increase monotonically with temperature. For the $HoNi_{2.6}Ga_{2.4}$-type low-temperature modification, both lattice parameters increase significantly with temperature, with a practically constant ratio c/a, however, the relative increase in a for the $CaCu_5$ type is much more pronounced than for c, resulting in a decreasing ratio c/a [see Fig. 5(a)]. Reasons for this behavior may partly be found (a) in the difference of the Ce valence in the two structure types (note, however, that we observed no variation of the cerium valence as a function of temperature; see Sec. III F) as well as (b) in the altered Ni-Ce,Ga bonding as monitored by the subtle changes in the tetrakaidecahedral coordination around the nickel atoms in the two structure modifications (see Sec. III B).

For the analysis of the volume variation with temperature, given by $\varepsilon_V=(V_{(T)}-V_0)/V_0$ with $V_0=V(4.2$ K)

we assume that ε_V is a sum consisting of an electronic and a phonon contribution

$$\varepsilon_V=\varepsilon_{el}+\varepsilon_{ph} , \quad (1)$$

where ε_{el} is given by

$$\varepsilon_{el}=K_2T^2 . \quad (2)$$

Within the Debye model the expression for phonon contribution to the thermal expansion reads

$$\varepsilon_{ph}(T)=K_1TD(\Theta_D/D) \quad (3)$$

with $D(z)=3/z\int_0^z(x^3/e^x-1)dx$. From a least-squares fit of Eq. (1) to the experimental data we determined the Debye temperatures and the values of K_1 and K_2. This fit procedure revealed that the prefactors K_2 which are expected to be proportional to the γ value of the electronic specific heat are too uncertain to draw further conclusions. Neglecting the electronic part in the fit procedure, the Debye temperature and the values of K_1 are shown in Fig. 5(b). The solid lines in Fig. 5(b) show the fit of Eq. (3) to the experimental data. Comparing the corresponding Debye temperatures and the prefactors K_1 (which also depend on the Debye temperature) it clearly follows that the lattice of the $HoNi_{2.6}Ga_{2.4}$-type modification is considerably softer than the lattice of the $CaCu_5$-type structure. The temperature variation of the thermal expansion, approximated by the following polynomial

$$L_P(T)=L_P(0)[1+\alpha T+\beta T^2+\gamma T^3] \quad (4)$$

is given in Table IV and Fig. 5(a).

D. The solid solutions $Ce_{1-x}(Y,La)_x(Ni_{1-y}Ga_y)_5$, $x=0.33, 0.67$ $y=0.2, 0.4$, and 0.47

Due to the lack of external pressure equipment, we attempted to collect relevant information on the pressure dependence of the physical properties by simulation of a chemical internal pressure on the cerium atom when

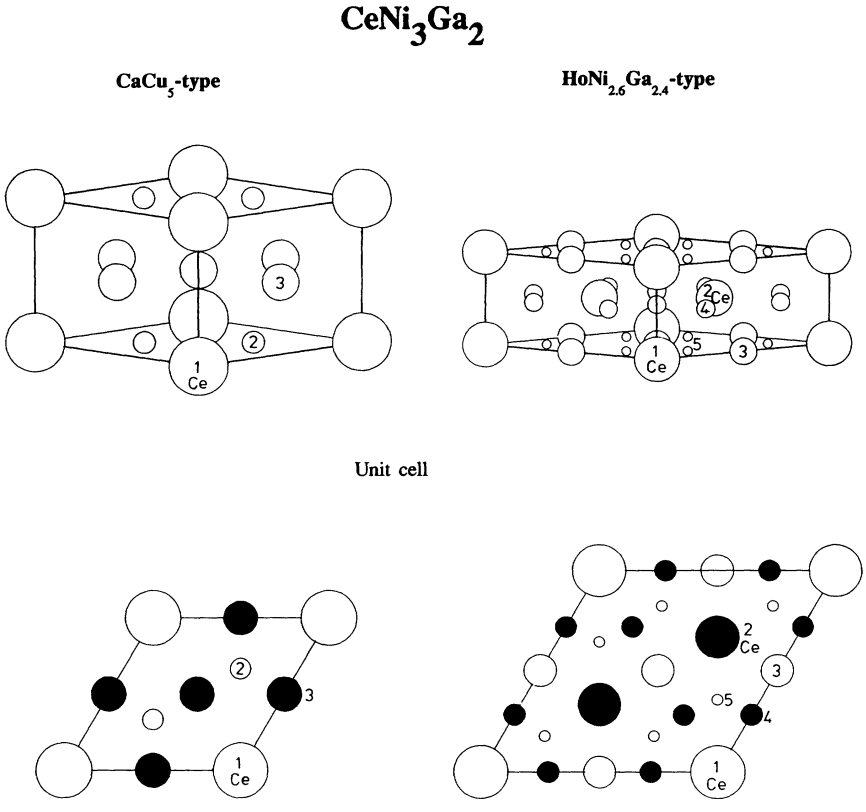

FIG. 4. Unit cell and projection along [001] for the $CaCu_5$- and the $HoNi_{2.6}Ga_{2.4}$-type (disordered YNi_2Al_3-type).

Atom-No.	Wyckoff-symbol	Atom	x	y	z
1	1a	Ce	0	0	0
2	2c	Ni	1/3	2/3	0
3	3g	*	1/2	0	1/2

Atom-No.	Wyckoff-symbol	Atom	x	y	z
1	1a	Ce	0	0	0
2	2d	Ce	1/3	2/3	1/2
3	3f	*	1/2	0	0
4	6k	*	0.2825	0	1/2
5	6l	Ni	0.1785	0.3570	0

*0.67 Ga + 0.33 Ni

one-third of them are replaced by smaller yttrium (positive internal pressure) or by larger lanthanum (negative internal pressure). The observed volume changes naturally are expected to vary with the volume ratio V_{Ce}/V_{RE}.

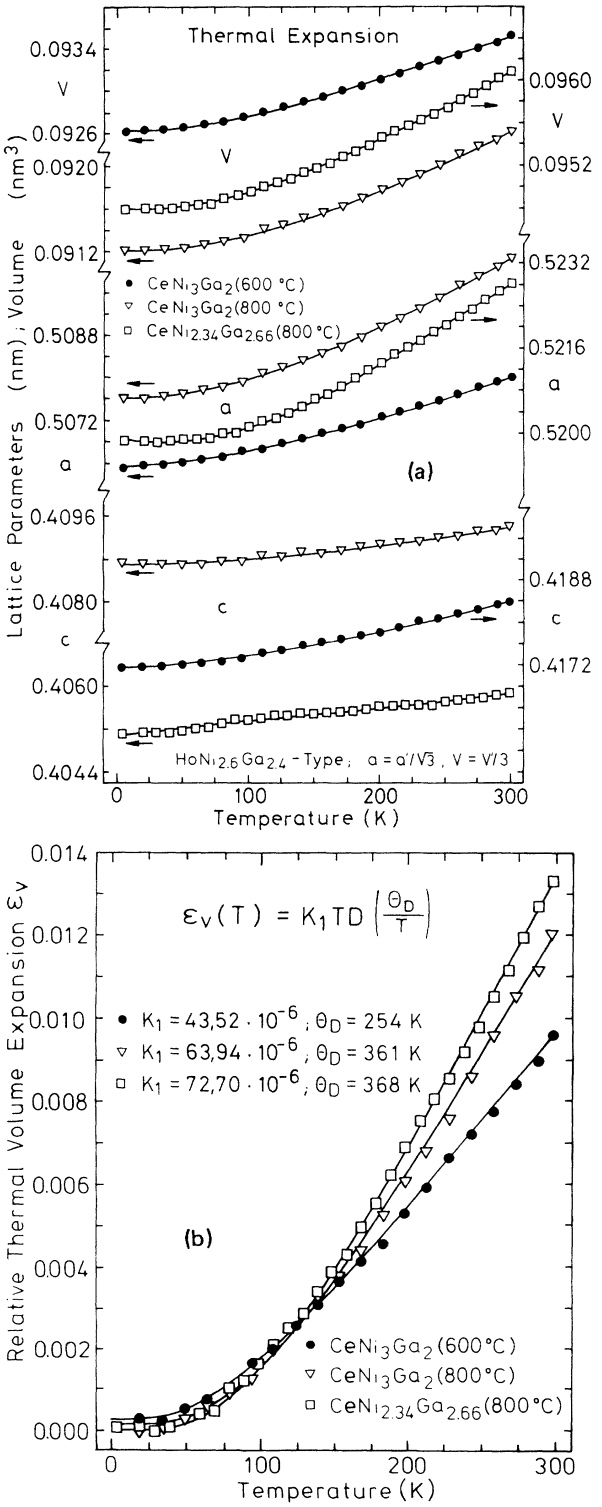

FIG. 5. (a) Thermal expansion of the two modifications of $CeNi_3Ga_2$ and of $CeNi_{2.34}Ga_{2.66}$ with the $CaCu_5$ type. (b) Relative thermal volume expansion and least-squares fit with the Debye formula; K_1 in K^{-1}.

Interestingly these dependences were observed to be practically linear for all values of x,y investigated (see Fig. 6). This is particularly surprising for both the structure modifications of $CeNi_3Ga_2$, for which XAS resulted in significantly different cerium valences (see Sec. III F). As far as the thermodynamic stability of the $HoNi_{2.6}Ga_{2.4}$-type (disordered YNi_2Al_3-type) low-temperature modification is concerned, we observe for both types of substitution an increase of thermodynamic stability, i.e., a shift of the transition point to slightly higher temperatures.

E. Magnetism

The magnetic behavior of the intermetallic compound $CeNi_5$ has been characterized by an enhanced isotropic susceptibility with a maximum in χ versus T around 100 K (Fig. 7). Based on a detailed investigation[19,20] including polarized-neutron scattering, the magnetization is localized exclusively on the Ni atoms, whereas the nonmagnetic Ce ground state is due to strong $4f$ hybridization effects. The maximum in the susceptibility was found to arise from spin fluctuations due to hybridization, which are characteristic for systems close to the onset of magnetism. This picture is supported by recent band-structure calculations for $CeNi_x$.[21,22]

The partial substitution of nickel by gallium has a pronounced influence on the magnetic behavior. As can be seen in Fig. 7 for $CeNi_3Ga_2$ with the $CaCu_5$ type, the susceptibility is independent of temperature for $150 < T < 500$ K. This behavior is typically observed for the whole solid solution $Ce(Ni_{1-x}Ga_x)_5$ and was also reported in an earlier investigation of $Ce(Ni_{1-x}Ga_x)_5$ for two alloys $x=1$ and 1.175 by Koterlin *et al.*,[8] however, their absolute values of χ_g are smaller when compared with our data (see Table V).

The magnetism of these alloys is obviously governed by a nonmagnetic ground state of the cerium atoms. Furthermore, the admixture of the Ga p states seems to reduce the intraatomic exchange interaction responsible for the enhanced Pauli paramagnetism for binary $CeNi_5$. The decreased hybridization in turn may cause a more-localized behavior of the Ce atom. Upon lowering the temperature the susceptibilities increase. The effective moments derived for the low-temperature regime are small [$< 1\mu_B$, (Table V)]. The observed susceptibility for $CeNi_3Ga_2$ ($CaCu_5$ type) at elevated temperatures ($T > 500$ K) is again a function of temperature. The calculated average moment (Table V) of $1.4\mu_B$ can be interpreted in the scope of the interconfiguration fluctuation model[22] as the partial occupation of the $4f$ levels lying closely above E_F. This argumentation is in good agreement with the theoretical occupation numbers of $n_{4f} \sim 1$ electron per atom in $CeNi_x$ compounds[21] and the L_{III}-absorption data (see below). The magnetic data of the low-temperature modification of $CeNi_3Ga_2$ with the $HoNi_{2.6}Ga_{2.4}$ type, however, show a remarkable difference when compared with the $CaCu_5$ type (Fig. 7). The magnetic susceptibility of the latter compound can be accounted for by a Curie-Weiss law and a temperature-independent Pauli contribution χ_0,

TABLE IV. Thermal expansion of the lattice parameters of $CeNi_3Ga_2$, ($HoNi_{2.6}Ga_{2.4}$ type and $CaCu_5$ type) and $CeNi_{2.34}Ga_{2.66}$, ($CaCu_5$ type).

	$HoNi_{2.6}Ga_{2.4}$ type $CeNi_3Ga_2$			$CaCu_5$ type $CeNi_3Ga_2$			$CaCu_5$ type $CeNi_{2.34}Ga_{2.66}$		
Thermal expansion: $L_P(T)=L_P(0)[1+\alpha T+\beta T^2+\gamma T^3]$;	a	c	V	a	c	V	a	c	V
$L_P(0)$[a]	0.8770	0.4172	0.2779	0.5076	0.4087	0.091 20	0.5199	0.4051	0.094 80
$10^6\alpha$ [K^{-1}]	1.376	0.840	3.579	−0.592	−1.483	−2.665	−8.687	8.993	−8.391
$10^8\beta$ [K^{-2}]	5.381	5.369	16.14	8.751	4.110	21.60	15.13	−1.817	28.44
$10^{11}\gamma$ [K^{-3}]	−7.211	−7.981	−22.32	−9.170	−5.921	−24.05	−19.64	3.352	−35.68

[a] L_P in nm; V in nm^3.

$$\chi=\chi_0+C/(T+\Theta_p)\,, \tag{5}$$

where C is the Curie constant and Θ_p is the paramagnetic Curie temperature (see solid line in Fig. 7).

The deduced magnetic moment $\mu_{\text{eff}}\sim 2\mu_B$/f.u., assuming a zero-moment contribution from the (Ni,Ga) sublattice, corresponds to an intermediate valence state of $Ce^{3.4+}$, thereby perfectly agreeing with XAS data (see Sec. III F). In the above picture this behavior could be understood schematically: the structural ordering, which effects the interatomic distances as well as the coordination leads to a narrowing of the $3d$ band and hence the Fermi level is moved towards the $4f$ band increasing the magnetic $4f$ contribution. For comparison we have also measured the isotypic $La(Ni_{1-x}Ga_x)_5$ compounds (see Tables V and VI); both samples appear to be temperature-independent Pauli paramagnets. Small upturns of χ versus T below 20 K may be due to impurity contributions. Finally the partial substitution of cerium by yttrium and lanthanum in the quaternary alloys $Ce_{1-x}R_x(Ni_{1-y}Ga_y)_5$ (see Table VI) does not affect their magnetic behavior indicating constant cerium valence within the rare-earth solid solutions (see also Sec. III F). The samples of the $CaCu_5$ type remain temperature-independent paramagnets, whereas for alloys with the $HoNi_{2.6}Ga_{2.4}$ type an average effective magnetic moment $\mu_{\text{eff}}\cong 1.9\mu_B$ per cerium atom was derived.

Figure 8 shows the magnetization as a function of field at $T=1.5$ K for various concentrations of this series. For the magnetization at 8 T, we obtained values much below $0.1\mu_B$/f.u., thus confirming the intermediate valence state of cerium. However, $CeNi_3Ga_2$ with the $HoNi_{2.6}Ga_{2.4}$ type behaves differently. For this compound, the magnetization at 8 T attains nearly $0.3\mu_B$/f.u. Such a value can be thought to originate from crystal-field effects which split the cerium $F_{5/2}$ state into three doublets. The impact of the crystal field on this compound is most likely seen also from the negative curvature of the inverse susceptibility of $CeNi_3Ga_2$, particularly below 50 K. All the investigated compounds show a smooth increase of the magnetization with increasing field, except $CeNi_{2.34}Ga_{2.66}$. The latter alloy is characterized by a small metamagnetic transition, thus indicating long-range magnetic order. The inset of Fig. 8 shows an Arrott plot for this concentration at different temperatures. Clearly visible is the change of behavior for the curve $T=34$ K. From this plot we conclude an antiferromagnetic order at $T_N=33$ K (see also inset Fig. 7) with rather small magnetic moments.

F. X-ray-absorption spectroscopy

For the light rare-earth elements, such as Ce, hybridization between the $4f$ and the conduction electrons becomes important, and an unoccupied $4f$ level in the initial state is lowered below the Fermi level in the final state, which can be occupied.[24] Such hybridization

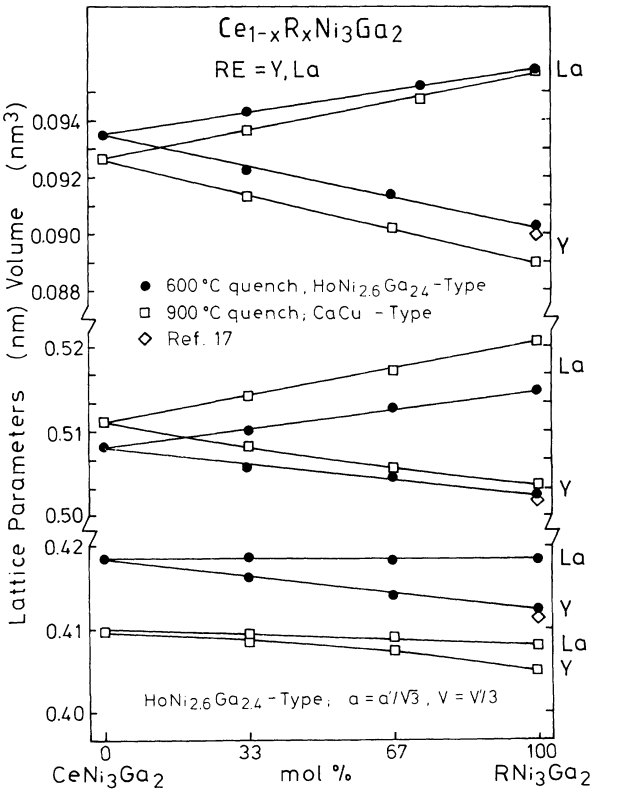

FIG. 6. Lattice parameters and volume of $Ce_{1-x}R_xNi_3Ga_2$ versus composition. Alloys were quenched from 600 and 900 °C.

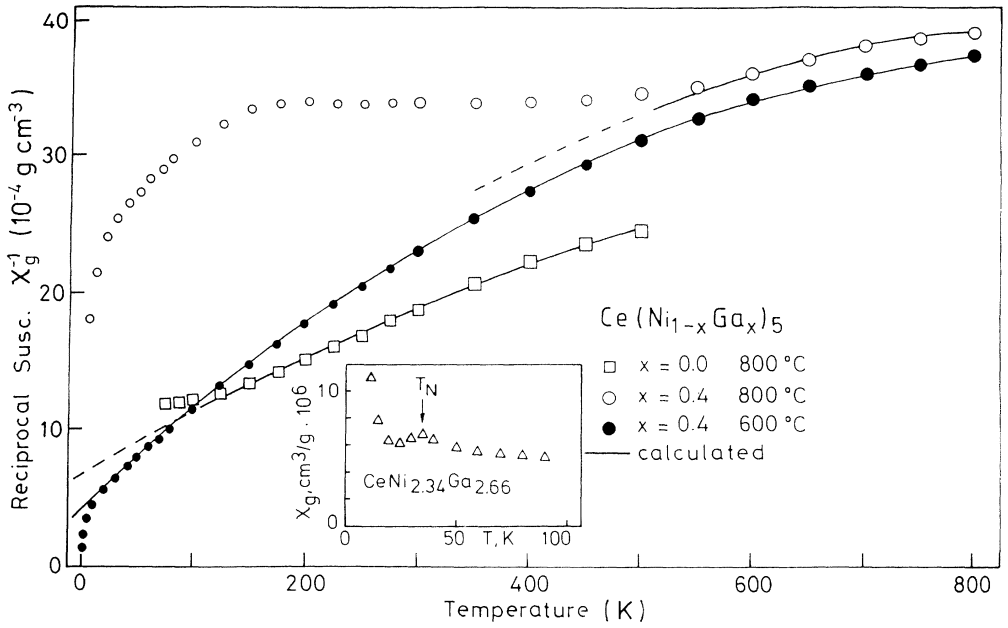

FIG. 7. $1/\chi$ versus T plot of some typical compounds of the section $Ce(Ni_xGa_{1-x})_5$. The inset shows the data for $CeNi_{2.34}Ga_{2.66}$ up to 90 K.

effects have been taken into account in the calculations of Gunnarson and Schönhammer.[25] To compare the valences obtained from a direct fit of the L_{III}-edge spectra, $\nu(Ce,L_{III})$, with those deduced from lattice parameters and magnetic measurements, the values ν_{Ce} have been calculated on the basis of the following transformation:

$$\nu_{Ce}=\{\nu(Ce,L_{III})-3\}/0.36+3\ . \tag{6}$$

Results are summarized in Figs. 9 and 10. Evaluation is based on the literature mean value of $\nu(Ce,L_{III})=3.36$ for the tetravalent $CeNi_5$,[26,27] which agrees with the probability of finding about 60% of $4f^1$ final states and 40% of $4f^0$ final states in a single Ce^{4+} configuration.[26] This is of special interest in the case of $CeNi_3Ga_2$ with the $HoNi_{2.6}Ga_{2.4}$-type structure, in which two Ce sites exist with the ratio $\frac{1}{2}$. In such a case, classical understanding of the structure, in which Ce ions are in $2d$ and $1a$ sites would give a valence of 3.33 if the corresponding Ce ions were trivalent and tetravalent respectively comparing well with the valence $\nu_{Ce}=3.28$. Similarly, two trivalent and one "tetravalent" ions ($0.6\times4f^1+0.4\times4f^0$) should give a valence $\nu(Ce,L_{III})=3.13$, which agrees with the experimental value of 3.10.

Within the accuracy of the L_{III} experiment, valences at

TABLE V. Magnetic data of ternary compounds $Ce(Ni_{1-x}Ga_x)_5$.

Compound	Temp. region of calcul. (K)	Structure type	μ_{eff} f.u. (μ_B)	Θ_p (K)	Ref.
$CeNi_5$	>100	$CaCu_5$	2.67	−154	a
			2.6	−120	23
$CeNi_{4.62}Ga_{0.38}$	<300	$CaCu_5$	0.9	−32	a
$GeNi_4Ga$	<150	$CaCu_5$	0.8	−35	a
	>150		TIP	$\chi_g=2.1\times10^{-6}$ cm^3/g	a
			TIP	$\chi_g=1.6\times10^{-6}$ cm^3/g	8
$CeNi_{3.05}Ga_{1.95}$	<100	$CaCu_5$	0.7	−30	a
$CeNi_3Ga_2$	>100	$HoNi_{2.6}Ga_{2.4}$	1.9	−36	a
	>500	$CaCu_5$	1.4	−28	a
$CeNi_{2.68}Ga_{2.32}$	<100	$CaCu_5$	0.4	−7	a
$CeNi_{2.34}Ga_{2.66}$	<100	$CaCu_5$	0.4	16[b]	a
$LaNi_4Ga$	5	$CaCu_5$	TIP	$\chi_g=4.4\times10^{-6}$ cm^3/g	a
$LaNi_3Ga_2$	5	$HoNi_{2.6}Ga_{2.4}$	TIP	$\chi_g=3.0\times10^{-6}$ cm^3/g	a

[a]This work.
[b]Antiferromagnetic order at $T_N=34$ K.

TABLE VI. Crystallographic data of $Ce_{1-x}(Y,La)_x(Ni_{1-y}Ga_y)_5$, $x=0.33, 0.67$ in the region $0.2 \leq y \leq 0.48$.

Alloy nominal comp.	Heat treatment	Structure type	Space group	Unit-cell dimensions (nm) a	c	V	c/a	Ref.
$Ce_{0.67}Y_{0.33}Ni_4Ga$	600 °C	$CaCu_5$	*P6/mmm*	0.4946(1)	0.4064(2)	0.08612	0.822	a
	800 °C	$CaCu_5$	*P6/mmm*	0.4941(1)	0.4072(1)	0.08609	0.824	a
$Ce_{0.67}Y_{0.33}Ni_3Ga_2$	600 °C	$HoNi_{2.6}Ga_{2.4}$	*P6/mmm*	0.8763(2)	0.4158(2)	0.2765	0.475	a
	800 °C	$CaCu_5$,	*P6/mmm*	0.5085(1)	0.4082(2)	0.09141	0.803	a
		$HoNi_{2.6}Ga_{2.4}$	*P6/mmm*	0.8757(2)	0.4165(4)	0.2766	0.476	a
	900 °C	$CaCu_5$	*P6/mmm*	0.5081(1)	0.4084(1)	0.09129	0.804	a
$Ce_{0.67}Y_{0.33}Ni_{2.68}Ga_{2.32}$	600 °C	$CaCu_5$,	*P6/mmm*	0.5186(1)	0.4062(1)	0.09462	0.783	a
		$HoNi_{2.6}Ga_{2.4}$	*P6/mmm*	0.8805(4)	0.4150(2)	0.2786	0.471	a
	800 °C	$CaCu_5$	*P6/mmm*	0.5142(1)	0.4063(1)	0.09302	0.790	a
$Ce_{0.33}Y_{0.67}Ni_3Ga_2$	600 °C	$HoNi_{2.6}Ga_{2.4}$	*P6/mmm*	0.8745(2)	0.4138(2)	0.2741	0.473	a
	900 °C	$CaCu_5$	*P6/mmm*	0.5054(1)	0.4076(3)	0.09015	0.806	a
$Ce_{0.67}La_{0.33}Ni_4Ga$	600 °C	$CaCu_5$	*P6/mmm*	0.4991(1)	0.4078(3)	0.08795	0.817	a
	800 °C	$CaCu_5$	*P6/mmm*	0.4962(1)	0.47079(1)	0.08696	0.822	a
$Ce_{0.67}La_{0.33}Ni_3Ga_2$	600 °C	$HoNi_{2.6}Ga_{2.4}$	*P6/mmm*	0.8834(3)	0.4185(1)	0.2828	0.474	a
	800 °C	$CaCu_5$,	*P6/mmm*	0.5140(1)	0.4090(2)	0.09357	0.796	a
		$HoNi_{2.6}Ga_{2.4}$	*P6/mmm*	0.8856(−)	0.4194(−)	0.2848	0.474	a
	900 °C	$CaCu_5$	*P6/mmm*	0.5140(1)	0.4091(1)	0.09360	0.796	a
$Ce_{0.67}La_{0.33}Ni_{2.68}Ga_{2.32}$	600 °C	$CaCu_5$,	*P6/mmm*	0.5208(2)	0.4068(3)	0.09554	0.781	a
		$HoNi_{2.6}Ga_{2.4}$	*P6/mmm*	0.8842(3)	0.4193(3)	0.2839	0.474	a
	800 °C	$CaCu_5$	*P6/mmm*	0.5193(1)	0.4077(1)	0.09523	0.785	a
$Ce_{0.33}La_{0.67}Ni_3Ga_2$	600 °C	$HoNi_{2.6}Ga_{2.4}$	*P6/mmm*	0.8879(2)	0.4180(2)	0.2853	0.471	a
	900 °C	$CaCu_5$	*P6/mmm*	0.5169(1)	0.4089(2)	0.09461	0.791	a
YNi_3Ga_2	600 °C	$HoNi_{2.6}Ga_{2.4}$	*P6/mmm*	0.8708(2)	0.4124(1)	0.2708	0.474	a
				0.8700	0.4115	0.2697	0.473	17
	900 °C	$CaCu_5$	*P6/mmm*	0.5036(0)	0.4049(1)	0.08894	0.804	a
$LaNi_3Ga_2$	900 °C	$CaCu_5$	*P6/mmm*	0.5205(1)	0.4079(1)	0.09571	0.784	a

[a]This work.

room temperature and low temperature (~ 10 K) do not change much, as generally observed in Ce-based materials in which this temperature dependence is weak in a mixed-valence system or zero in "saturated" valence compounds.[28] To our knowledge, the valence change between 280 and 10 K observed in $CeNi_{2.34}Ga_{2.66}$ [Fig. 10(a)] is larger than in any other system. Low temperature x-ray diffraction ascertains that no crystallographic transition takes place between room temperature and 10 K. This is in agreement with our x-ray absorption near-edge structure (XANES) results in the range 10–60 eV higher than the edge, which is sensitive to the chemical

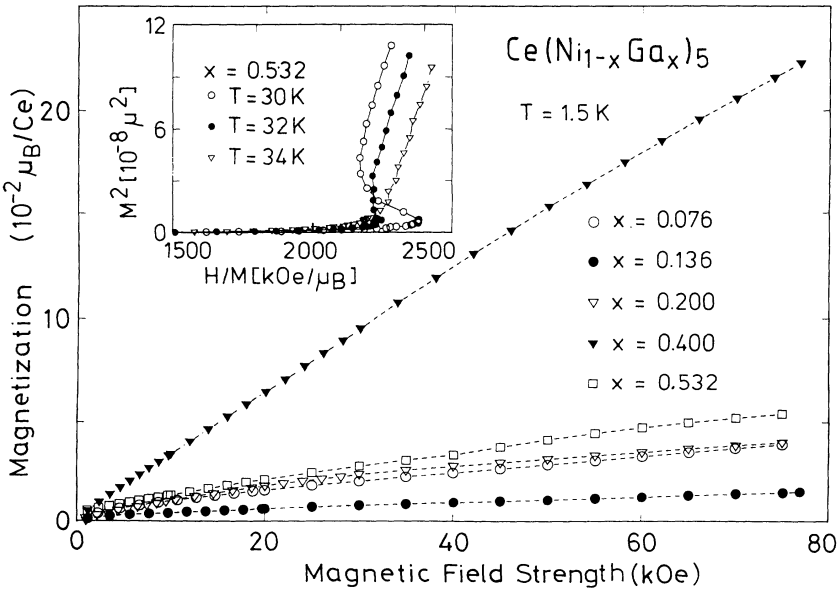

FIG. 8. Magnetization versus magnetic field strength for several compounds of the section $Ce(Ni_xGa_{1-x})_5$ quenched from 600 °C; alloys with $x=0.076$, 0.136, 0.2, and 0.532 are $CaCu_5$ type, $x=0.4$ is $HoNi_{2.6}Ga_{2.4}$ type. The inset shows the data as H/M versus M^2 for $CeNi_{2.34}Ga_{2.66}$ at several temperatures.

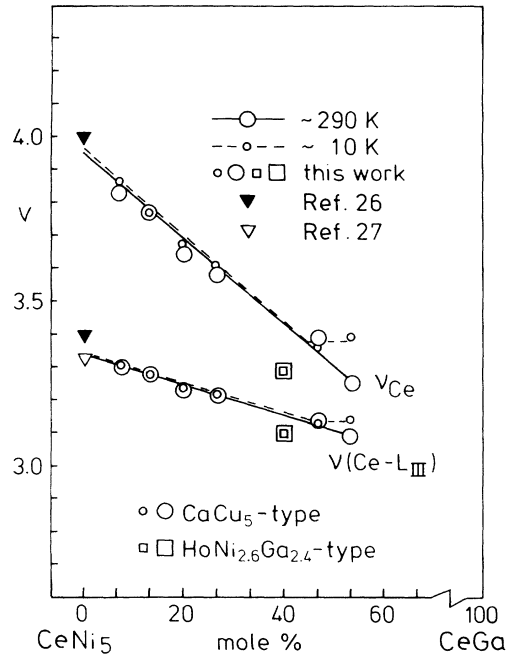

FIG. 9. $\nu(\mathrm{Ce}-L_{\mathrm{III}})$ and ν_{Ce} versus Ga concentration in $\mathrm{Ce(Ni_{1-x}Ga_x)_5}$.

environment[29] and does not show any modification between room temperature and 10 K [see Fig. 10(b)]. Further L_{III}-edge measurements versus temperature [see inset in Fig. 10(a)] indeed revealed a change in the Ce valence commencing at about 80 K towards higher temperatures. This behavior is reflected in a significant change of slope for the temperature dependences of the unit-cell dimensions [see Fig. 5(a)] of $\mathrm{CeNi_{2.34}Ga_{2.66}}$ and isostructural $\mathrm{CeNi_3Ga_2}$. The XAS data for substituted alloys $\mathrm{Ce_{1-x}(Y,La)_xNi_3Ga_2}$ in both structure modifications did not exhibit any significant variation for the cerium valence with respect to the $\mathrm{CeNi_3Ga_2}$-based alloys in correspondence with the linear variation of the unit-cell parameters as well as with the magnetic characterization (see Secs. III D and III E).

G. Electrical resistivity

Figure 11 shows the temperature-dependent electrical resistivity, $\rho(T)$, of $\mathrm{CeNi_5}$, $\mathrm{CeNi_4Ga}$, and for both modifications of $\mathrm{CeNi_3Ga_2}$. A representation, normalized to the respective room-temperature resistivity, is chosen to emphasize the crossover behavior when proceeding from $\mathrm{CeNi_5}$ to $\mathrm{CeNi_3Ga_2}$. While $\rho(T)$ of $\mathrm{CeNi_5}$ shows a smooth increase with rising temperatures, resembling the behavior found recently by Gignoux *et al.*[9] or Koterlin *et al.*,[8] the increasing content of Ga causes a quite dramatic change of the temperature-dependent resistivity. $\mathrm{CeNi_3Ga_2}$, exhibiting the $\mathrm{HoNi_{2.6}Ga_{2.4}}$ type of structure, is characterized by a broad range with rising resistivity values for lowering the temperature. Such a behavior is well known for Kondo-type scattering processes, which usually dominate the behavior of Ce compounds with almost integer valency. Indeed, $\mathrm{CeNi_3Ga_2}$ with the partially ordered $\mathrm{HoNi_{2.6}Ga_{2.4}}$ type is just that compound of the series which is, in comparison to the $\mathrm{CaCu_5}$-type high-temperature phase, much closer to a trivalent state of Ce (see Sec. III F). To demonstrate this behavior in a more quantitative way we describe the resistivity data of this compound, assuming the temperature-independent residual resistivity (ρ_0), the phonon contribution, (ρ_{Ph}), which according the Bloch-Grüneisen model is linear at elevated temperatures, and the Kondo interaction term showing a negative logarithmic temperature dependence. A least-squares fit according to this model is additionally shown in Fig. 11 as a full line for $\mathrm{CeNi_3Ga_2}$ giving satisfactory agreement with the experimental data. Deviations occurring have to be attributed most likely to the crystal-field splitting of the $F_{5/2}$ ground state of the Ce ion.

$\mathrm{CeNi_3Ga_2}$ with the $\mathrm{CaCu_5}$-type structure shows a less pronounced behavior when compared with the low-temperature modification ($\mathrm{HoNi_{2.6}Ga_{2.4}}$ type). This is referred, at least partly to the valency of this configuration being in a much more intermediate valence state than that of the $\mathrm{HoNi_{2.6}Ga_{2.4}}$ type. Consequently, the Kondo-type interaction is less dominant in the observed temperature range. Although the Ce ions occupy a regular sublattice in these compounds, expected coherence effects, such as a strong decrease of $\rho(T)$ at low temperatures, are not observed. This is explained from the disorder of the surrounding Ga and Ni ions which prevent the formation of Bloch waves of the conduction electrons at the lowest temperatures; hence, the absolute resistivity values remain large.

H. Specific-heat measurements

Figure 12 shows the temperature-dependent specific heat, $C_p(T)$, for $\mathrm{CeNi_4Ga}$ and for both modifications of $\mathrm{CeNi_3Ga_2}$ down to 1.5 K. Small humps around 6 K indicate traces of cerium oxide which, however, do not essentially change the observed $C_p(T)$ behavior. As the value of the valence decreases towards the trivalent state of Ce, the heat capacity of the compounds rises. The specific-heat dependence in the low-temperature range for both compounds $x=0.4$ indicates that either a magnetic phase transition occurs well below 1.5 K or strongly temperature-dependent specific-heat data have to be anticipated. Possible mechanisms for the latter are short-range order effects above a magnetic phase transition, strong correlations frequently observed in Ce compounds or Kondo interaction. The inset of Fig. 12 shows C_p/T versus T^2. For both modifications of $\mathrm{CeNi_3Ga_2}$, C_p/T strongly rises as the temperature is lowered. For $\mathrm{CeNi_3Ga_2}$ with the $\mathrm{HoNi_{2.6}Ga_{2.4}}$-type structure a value of more than 400 mJ/mol K^2 is attained at $T=1.5$ K. Even a high-temperature extrapolation of C_p/T versus T^2 yields a value of about 100 mJ/mol K^2, much larger than the respective values of $\mathrm{CeNi_5}$ ($\gamma=40.0$ mJ/mol K^2).[30] This enlargement of C_p/T when proceeding from $\mathrm{CeNi_5}$ to $\mathrm{CeNi_3Ga_2}$ is concomitant with the

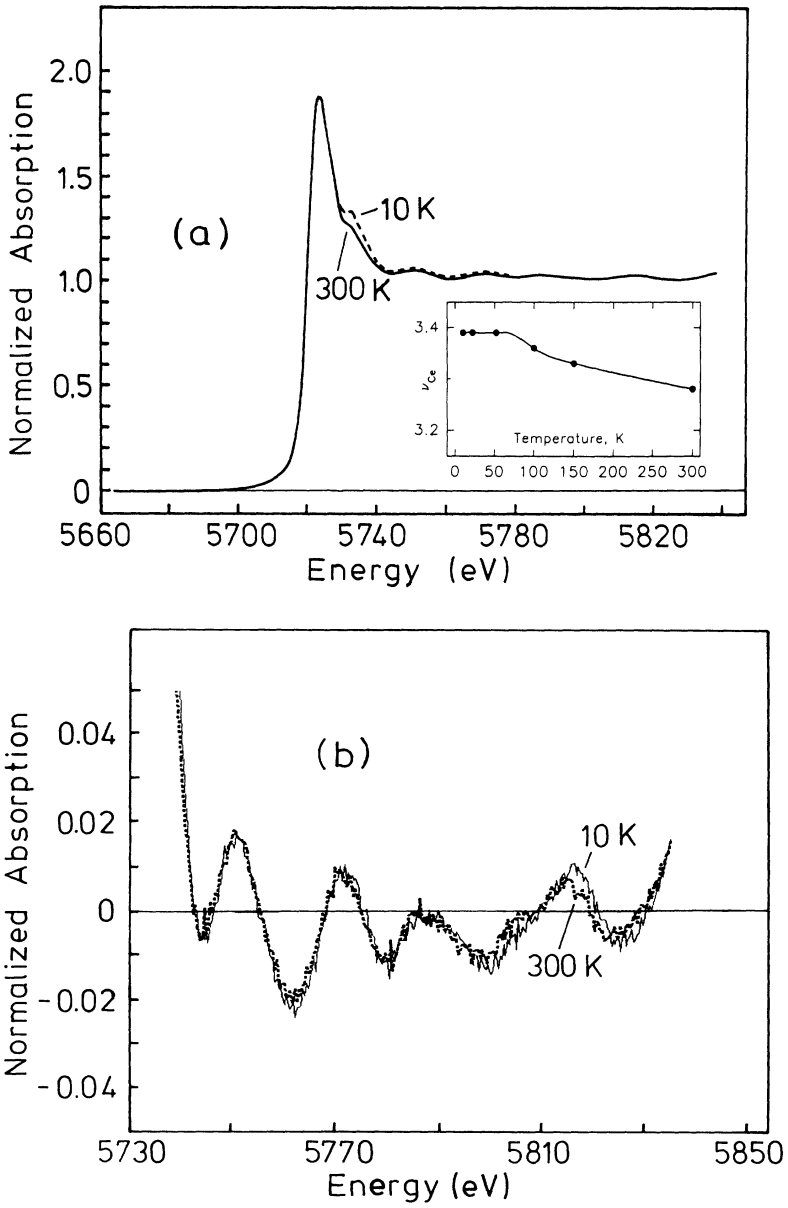

FIG. 10. (a) X-ray absorption versus energy (in eV) of the compound $CeNi_{2.34}Ga_{2.66}$ at ~10 K and RT. The inset shows the temperature dependence of ν_{Ce}. (b) The XANES region of the x-ray-absorption spectrum of $CeNi_{2.34}Ga_{2.66}$.

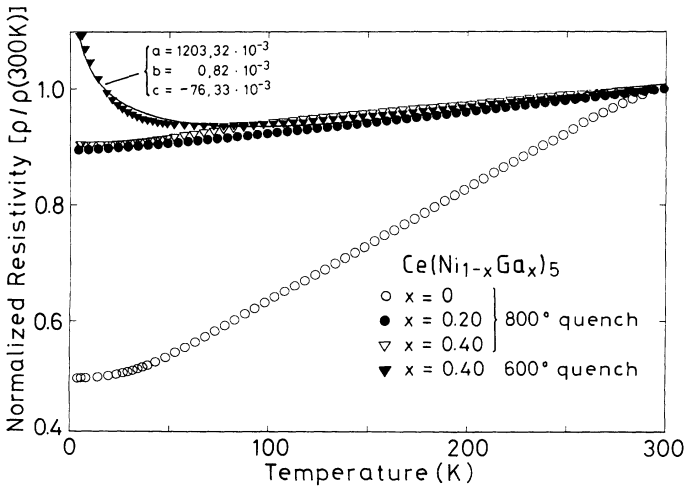

FIG. 11. Electrical resistivity $\rho(T)$ versus temperature for the compounds $CeNi_5$, $CeNi_4Ga$, and both modifications of $CeNi_3Ga_2$ and a least-squares fit according to $\rho = a + b \times T + c \times \ln(T)$ model for $CeNi_3Ga_2$ with the $HoNi_{2.6}Ga_{2.4}$ type.

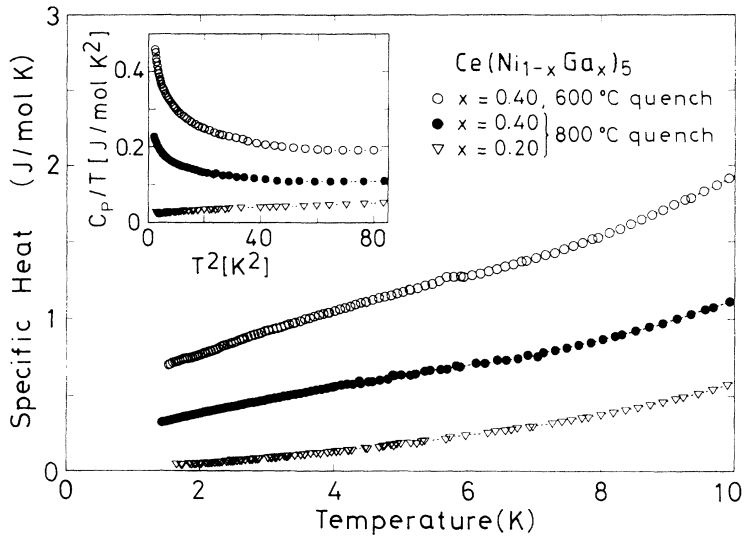

FIG. 12. Temperature-dependent specific heat $C_p(T)$ for $CeNi_4Ga$ and both modifications of $CeNi_3Ga_2$. The inset shows the data C_p/T versus T^2.

crossover from an almost tetravalent state in the former compound to a nearly trivalent state in the low-temperature modification of the latter compound. Susceptibility, L_{III} absorption edge studies and resistivity measurements have also confirmed this trend. In agreement with the resistivity results it is assumed that the Kondo effect is response for the strongly enhanced C_p/T values at low temperatures. Then the rapid rise of C_p/T below 10 K follows from the formation of a narrow, many-body resonance near the Fermi energy. The origin of this resonance is thought to descend from the singlet formation due to the Kondo effect. In order to take into account the removed spin and orbital degrees of freedom, a strongly temperature-dependent density-of-states peak develops slightly above the Fermy energy. Considering solutions of the Coqblin-Schrieffer model, which satisfactorily describe systems in an almost trivalent state, the characteristic temperature T_K in the crystal-field ground state is of the order of 10 K as an upper limit. The latter value is confirmed also from the observed paramagnetic Curie temperature Θ_P, which is -35 K. Depending on the model, Θ_P is related to T_K by $T_K = m|\Theta_P|$, where m ranges between 0.25 and 1.[31] However, it should be noted that systems, exhibiting statistical disorder in the crystallographic unit cell possibly yield spin-glass behavior, in spite of the fact that the magnetic Ce ions form a regular sublattice. Such systems are known as NMAD spin glasses[32] and can be therefore a source of large specific-heat values at low temperatures. In order to discriminate these mechanism reliably, measurements below 1 K in the present series would be very helpful.

IV. CONCLUSION

The alloy system $Ce(Ni_{1-x}Ga_x)_5$ reveals a continuous solid solution up to $x \sim 0.6$ which crystallizes with the $CaCu_5$ type at 800 °C but reveals the formation of a partially ordered low-temperature modification around $CeNi_3Ga_2$ with the $HoNi_{2.6}Ga_{2.4}$ type below a maximum congruent transition point at $T \cong 770$ °C. Physical properties are significantly different for the two structure modifications, such as magnetic susceptibility, field-dependent isothermal magnetization, specific heat, thermal expansion, electrical resistivity, XAS, and XANES.

While the $CaCu_5$-type solid solution on Ni/Ga substitution is characterized by a continuous filling of the Ni-3d band causing a reduction of 3d magnetism, the simultaneous shift in E_F towards the $4f^1$ state results in a growing magnetic contribution of the Ce-4f band. These characteristic changes in the magnetic state of cerium are obvious particularly from L_{III}-absorption measurements, which indicate a crossover from almost tetravalent cerium in $CeNi_5$ towards intermediate valence ($\nu_{Ce} = 3.25$ at RT) in $CeNi_{2.34}Ga_{2.66}$.

The low-temperature modification $CeNi_3Ga_2$ with the $HoNi_{2.6}Ga_{2.4}$ type is much closer to a Ce-trivalent state than the $CaCu_5$-type high-temperature phase. Considering the Curie-Weiss behavior of the magnetic susceptibility, the Ni contribution in addition seems to become less important. The pronounced tripositive behavior leads to Kondo-type interactions, which can be deduced from negative logarithmic contributions to the electrical conductivity or from enhanced values of the electronic contribution to the specific heat. The latter quantity attains a value of more than 400 mJ/mol K^2 at $T = 1.5$ K, at least more than one order of magnitude larger than that of simple metals and compounds.

ACKNOWLEDGMENTS

This research was sponsored by the Austrian Science Foundation (FWF) under Contracts No. P8218 and P8913-TEC. H. Flandorfer and C. Godart are grateful to the Austrian Academic Exchange Service (ÖAD) for financial support at CNRS-LCMTR in Meudon, and at the Institut für Physikalische Chemie in Wien, respectively (project A11).

*Author to whom correspondence should be addressed.

[1]N. Grewe and F. Steglich, in *Handbook of the Physics and Chemistry of Rare Earth,* edited by K. A. Gschneidner, Jr., and L. R. Eyring (Elsevier Science, Amsterdam, 1991), Vol. 14, Chap. 97, p. 343.

[2]P. Fulde, J. Keller, and G. Zwicknagl, Solid State Phys. **41**, 1 (1988).

[3]C. Geibel, S. Thies, D. Kaczorowski, A. Mehner, A. Granel, B. Seidel, U. Ahlheim, R. Helfrich, K. Peterson, C. D. Bredl, and F. Steglich, Z. Phys. B **83**, 305 (1991).

[4]C. Geibel, C. Schank, S. Thies, H. Kitazawa, C. D. Bredl, A. Böhm, M. Raw, A. Granel, R. Caspary, R. Helfrich, U. Ahlheim, G. Weber, and F. Steglich, Z. Phys. B **84**, 1 (1991).

[5]E. Bauer, Adv. Phys. **40**, 417 (1991).

[6]E. I. Gladischevsky, O. I. Bodak, and V. K. Pecharsky, in *Handbook on the Physics and Chemistry of Rare Earth,* edited by K. A. Gschneidner, Jr., and L. R. Eyring (Elsevier Science, Amsterdam, 1990), Vol. 13, p. 1.

[7]Yu. N. Grin, Ya. P. Yarmolyuk, and V. K. Pecharsky, Izv. Akad. Nauk., SSSR, Met. **3**, 213 (1983).

[8]M. D. Koterlin, O. I. Babich, B. S. Morokhivskii, G. Ya. Len', R. V. Lutsiv, and Yu. N. Grin, Sov. Phys. Solid State **29**(3), 542 (1987).

[9]M. D. Koterlin, O. I. Babich, B. S. Morokhivskii, M. B. Konyk, and R. V. Lutsiv, Sov. Phys. Solid State **30**(5), 873 (1988).

[10]K. E. Johansson, J. Phys. E **13**, 1289 (1980).

[11]D. B. Wiles and R. A. Young, J. Appl. Crystallogr. **14**, 151 (1981), (LNS/ILL version, J. Rodriguez).

[12]A. Lindbaum and M. Rotter (unpublished).

[13]J. Röhler, J. Magn. Magn. Mater. **47&48**, 175 (1985).

[14]D. Bonnin, P. Kaiser, J. Desbarres, and C. Fretigny (unpublished).

[15]O. S. Zarechnjuk and R. M. Rykhal, Vestn. Lviv. Univ. Ser. Khim. **23**, 45 (1981).

[16]R. M. Rykhal, O. S. Zarechnjuk, and Ja. I. Kuten, Dopov. Akad. Nauk Ukr. RSR, Ser. A **12**, 1136 (1978).

[17]M. A. Fremy, D. Gignoux, J. M. Moreau, D. Paccard, and L. Paccard, J. Less-Comm. Metals **106**, 251 (1985).

[18]K. H. J. Buschow, M. Brouha, H. J. van Daal, and A. R. Miedema, in *Valence Instabilities and Related Narrow-Band Phenomena, Proceedings of an International Conference, Rochester, New York, 1976,* edited by R. D. Parks (Plenum, New York, 1977), p. 125.

[19]D. Gignoux, F. Givord, R. Lemaire, H. Launois, and F. Sayetat, J. Phys. (Paris) **43**, 173 (1982).

[20]D. Gignoux, F. Givord, R. Lemaire, H. Launois, and F. Tasset, J. Magn. Magn. Mater **50**, 53 (1985).

[21]L. Nordström, M. S. S. Brooks, and B. Johnansson, Phys. Rev. B **46**, 3458 (1992).

[22]S. Cabus, K. Gloos, H. Gottwick, S. Horn, M. Klemm, J. Kübler, S. Steglich, and R. D. Parks, Solid State Commun. **51**, 909 (1984).

[23]K. H. J. Buschow, in *In Ferromagnetic Materials,* edited by E. P. Wohlfahrt (North-Holland, Amsterdam, 1980), p. 383.

[24]G. Krill, J. P. Kappler, N. Wetta, E. Beaurepaire, D. Malterre, and C. Godart, *Theoretical and Experimental Aspects of Valence Fluctuations,* edited by L. C. Gupta and S. C. Malik (Plenum, New York, 1987), p. 205.

[25]O. Gunnarsson and K. Schönhammer, Phys. Rev. B **31**, 4815 (1985).

[26]G. Krill, J. P. Kappler, A. Meyer, L. Abadly, and M. F. Ravet, in *Valence Fluctuations in Solids,* edited by L. M. Falicov, W. Hanke, and M. B. Maple (North-Holland, Amsterdam, 1981), p. 435.

[27]K. R. Bauchspiess, W. Boksch, E. Holland-Moritz, H. Launois, R. Pott, and D. Wohlleben, in *Valence Fluctuations in Solids* (Ref. 26), p. 417.

[28]E. Beaurepaire, J. P. Kappler, J. Sereni, C. Godart, and G. Krill, in *Proceedings of the International Conference XAFS VI, New York, 1990,* edited by S. S. Hasnain (Harwood, New York, 1991).

[29]P. J. Durham, J. B. Pendry, and C. H. Hodges, Solid State Commun. **38**, 159 (1981).

[30]S. Nasu, H. H. Neumann, N. Marzouk, R. S. Craig, and W. E. Wallace, J. Phys. Chem. Solids **32**, 2779 (1971).

[31]G. Grüner and A. Zawadowsky, in *Progress in Low Temperature Physics,* edited by D. F. Brewer (North-Holland, Amsterdam, 1978), Vol. VII B, p. 591.

[32]K. A. Gschneidner, Jr., J. Tang, S. K. Dar, and A. Goldman, Physica B **163**, 507 (1990), and references cited therein.